BIOCHEMISTRY
including biophysical chemistry & molecular biology

Article

pubs.acs.org/biochemistry

Structural and Dynamic Features of Cold-Shock Proteins of *Listeria monocytogenes*, a Psychrophilic Bacterium

Juho Lee,[†] Ki-Woong Jeong,[†] Bonghwan Jin,[†] Kyoung-Seok Ryu,[‡] Eun-Hee Kim,[‡] Joong-Hoon Ahn,[†] and Yangmee Kim*[,†]

[†]Department of Bioscience and Biotechnology, Bio/Molecular Informatics Center, Konkuk University, Seoul 143-701, South Korea
[‡]Magnetic Resonance Team, Korea Basic Science Institute, Ochang, Chungbuk 363-883, South Korea

ABSTRACT: Cold-shock proteins (Csps), proteins expressed when the ambient temperature drops below the growth-supporting temperature, bind to single-stranded nucleic acids and act as RNA chaperones to regulate translation. *Listeria monocytogenes* is a psychrophilic food-borne pathogen that is problematic for the food industry. Structures of Csps from psychrophilic bacteria have not yet been studied. Despite dramatic differences in the thermostability of Csps of various thermophilic microorganisms, these proteins share a high degree of primary sequence homology and a high degree of three-dimensional structural similarity. Here, we investigated the structural and dynamic features as well as the thermostability of *L. monocytogenes* CspA (*Lm*-CspA). *Lm*-CspA has a five-stranded β-barrel structure with hydrophobic core packing and two salt bridges. When heptathymidine (dT_7) binds, values for the heteronuclear nuclear Overhauser effect and order parameters of residues in surface loop regions near nucleic acid binding sites increase dramatically. Moreover, Carr−Purcell−Meiboom−Gill experiments showed that slow motions observed for the nucleic acid binding residues K7, W8, F15, F27, and R56 disappeared in *Lm*-CspA-dT_7. *Lm*-CspA is less thermostable than mesophilic and thermophilic Csps, with a lower melting temperature (40 °C). The structural flexibility that accompanies longer surface loops and less hydrophobic core packing and a number of salt bridges and unfavorable electrostatic repulsion are likely key factors in the low thermostability of *Lm*-CspA. This implies that the large conformational flexibility of psychrophilic *Lm*-CspA, which more easily accommodates nucleic acids at low temperature, is required for RNA chaperone function under cold-shock conditions and for the cold adaptation of *L. monocytogenes*.

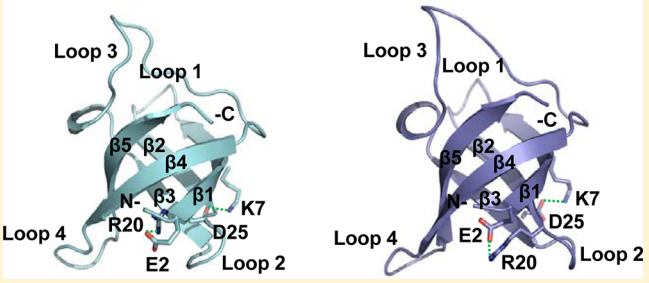

Bacteria have adapted to survive under extreme physical and chemical conditions. Living organisms that proliferate in such extreme environments, such as high or low temperature, high or low pressure, and/or extreme pH, are termed extremophiles. Bacteria have been classified on the basis of their "preferred" growth temperature (from high to low) as hyperthermophiles, thermophiles, mesophiles, and psychrophiles.[1,2] The adaptation of bacteria to sudden decreases in temperature reflects the downregulation of many cellular genes, such as those affecting the rate of synthesis of nucleic acids and proteins, the growth rate of cells, and fatty acid saturation.[3−7] Bacteria also respond by upregulating cold stress-response genes, such as cold-shock proteins (Csps), the RNA helicase DeaD, the DNA gyrase GyrA, the transcription factor NusA, and the translation factor InfB.[8−11]

Csps found in psychrophilic, mesophilic, thermophilic, and hyperthermophilic bacteria are structurally highly conserved. They have two nucleic acid binding motifs, ribonucleoprotein (RNP) 1 and 2, in which basic and aromatic residues form a nucleic acid-binding surface and contribute to the binding of single-stranded nucleic acids with micromolar to nanomolar dissociation constants. Csps act as RNA chaperones by binding single-stranded nucleic acids and destabilizing the secondary structure of mRNAs. Under low-temperature stress conditions, RNA is stabilized and forms a nonproductive secondary structure that interferes with transcription and translation. Csps melt RNA and destabilize this secondary structure, changing it to a single-stranded form; in doing so, they facilitate transcription and translation and thus act as a transcription antiterminator.[12−15] Csps are present in a wide range of bacteria, often in families of three (as in *Bacillus subtilis*) to nine (as in *Escherichia coli*) highly homologous members (>70% identical). Recently, Csps have been found in the thermophilic bacteria *Aquifex aeolicus* and *Thermotoga maritima*, indicating that they were present at the point of bacterial divergence and therefore are presumably evolutionarily old proteins.[9] The three-dimensional structures of bacterial Csps, including *E. coli* CspA (*Ec*-CspA),[16,17] *B. subtilis* Csps (*Bs*-CspB),[18−20] *Bacillus caldolyticus* Csps (*Bc*-Csp),[21,22] *T. maritima* Csps (*Tm*-Csp),[23] *Salmonella typhimurium* Csps (*St*-Csp),[24] and *Mycobacterium tuberculosis* Csps (*MTB*-Csp),[25] have been studied using X-ray crystallography and nuclear magnetic resonance (NMR)

Received: December 7, 2012
Revised: March 15, 2013
Published: March 18, 2013

 © 2013 American Chemical Society

spectroscopy. All of these Csps contain five antiparallel β-strands with an oligonucleotide/oligosaccharide-binding fold. An important feature of Csps structures is their many solvent-exposed aromatic residues, which directly bind single-stranded nucleic acids. Despite the high degree of conservation of structural features of Csps, experimental studies have revealed dramatic differences in the thermostabilities of these proteins, measured as unfolding or melting temperature (T_m). Mesophilic *Ec*-CspA unfolds at 60 °C at pH 7.5,[16,17] whereas *Bs*-CspB, Csps from another mesophilic bacterium, has a T_m of 52 °C.[19] Thermophilic *Bc*-Csp has a higher T_m of 77 °C.[22] *Tm*-Csp, which occurs in a species that grows optimally at 87 °C, appears to be even more thermostable, with a T_m of 80 °C.[23]

Listeria monocytogenes is a psychrophilic Gram-positive food-borne pathogen that poses public health risks as well as food safety challenges. It causes a food-borne illness responsible for more food poisoning fatalities than *Salmonella* or *E. coli* because it can proliferate at temperatures ranging from 4 to 45 °C. *L. monocytogenes* efficiently adapts and sometimes proliferates despite exposure to the low pH and elevated salt concentrations used in preserving ready-to-eat foods.[26] Given the challenges that these organisms introduce for ensuring food safety, an improved understanding of the role of Csps in the normal growth and stress adaptation of *L. monocytogenes* is a matter of particular interest.[27] However, less is known about the cold-shock characteristics of psychrophilic bacteria than mesophilic bacteria, such as *E. coli* and *B. subtilis*. Therefore, further studies are needed to unravel the thermodynamics and functions of psychrophilic Csps and determine their roles in the global, low-temperature regulatory system. Three Csp family proteins (CspA, CspB, and CspD) are found within the sequenced genome of *L. monocytogenes*, but their functions are not yet fully understood. Of these, CspA, hereafter termed *L. monocytogenes* CspA (*Lm*-CspA), functions under cold-stress conditions.[28]

The three-dimensional structures of Csps from thermophilic microorganisms, for example, their primary sequences, are highly similar despite the dramatic differences in the thermostabilities of these proteins noted above. Differences in thermostability among Csps might be closely related to the cold-shock adaptations of various bacteria. Structures of Csps from several hyperthermophilic and mesophilic bacteria have been reported, whereas structures of Csps from psychrophilic bacteria remain unavailable. Therefore, to understand the key factors that contribute to the thermostability of *Lm*-CspA, we investigated the solution structures of free *Lm*-CspA and the single-stranded nucleic acid [heptathymidine (dT_7)]-bound complex *Lm*-CspA-dT_7. Because flexibility in protein conformation plays a key role in molecular recognition and thus is essential for protein function, we also analyzed the dynamic properties of free *Lm*-CspA and *Lm*-CspA-dT_7 using NMR spin-relaxation techniques.

MATERIALS AND METHODS

Protein Expression, Isotopic Enrichment, Purification, and Site-Directed Mutagenesis. Wild-type *Lm*-CspA was constructed in a pET-11a vector, and the resulting plasmid was transduced into *E. coli* BL21(DE3) cells. Plasmid DNA was isolated from *E. coli* using a standard alkaline lysis mini-prep method.[29] Mutagenesis of the *Lm*-CspA variant was performed using the Muta-Direct Site Directed Mutagenesis Kit (Intron), and plasmid constructs of *Lm*-CspA variants containing mutations at positions 15 (F15A), 17 (F17A), and 27 (F27A) were cloned by polymerase chain reaction (PCR) using the synthetic oligonucleotide primer pairs 5′-gcagaaaaa-ggagcgggttttatcgaacgc-3′ (forward) and 5′-gcgttcgataaaacccgct-ccttttttctgc-3′ (reverse) for F15A, 5′-aaaggatttggtgcgatcgaacgcg-aaaac-3′ (forward) and 5′-gttttcgcgttcgatcgcaccaaatccttt-3′ (reverse) for F17A, and 5′-ggtgacgatgtagcggtacatttcagc-3′ (forward) and 5′-gctgaaatgtaccgctacatcgtcacc-3′ (reverse) for F27A, using *Lm*-CspA DNA as a template. PCR amplifications were performed using 10 fmol of template DNA, each primer at 1 μM, each deoxyribonucleotide triphosphate at 0.2 mM, and 2 μM Taq polymerase under the following thermocycling conditions: 18 cycles of denaturation at 94 °C (1 min), annealing at 54 °C (1 min), and primer extension at 72 °C (6 min). For expression of ^{1}H-, ^{15}N-, and ^{13}C-labeled *Lm*-CspA, *E. coli* BL21(DE3) cells were transformed with plasmids encoding *Lm*-CspA, then grown overnight as starter cultures, and collected by centrifugation. The resulting cell pellet was mixed with 200 mL of M9 minimal medium containing $^{15}NH_4Cl$ and [^{13}C]glucose (Cambridge Isotope Laboratories, Andover, MA) and 25 mg/L ampicillin and grown to an optical density at 600 nm (OD_{600}) of 0.8−1.0. The cell pellet from this culture was added to 1 L of the same medium and grown to an OD_{600} of 0.8−1.0. Protein expression was induced by addition of isopropyl β-D-thiogalactopyranoside and incubation at 10 °C for approximately 24 h. After being harvested, cell pellets were stored at −74 °C.

Pelleted cells were resuspended and lysed by ultrasonication in equilibrium buffer [6 mM Tris-HCl (pH 6.8), 2 mM dithiothreitol, and 2 mM ethylenediaminetetraacetic acid (EDTA)] and centrifuged at 28330*g*. The supernatant was loaded onto an anion exchange column with equilibrium buffer, and the protein was eluted using a buffer containing 300 mM NaCl (pH 6.8). Concentrated protein was purified using size-exclusion and hydrophobic-interaction chromatography. In general, the yield from 1 L of culture was 1−2 mg.

Circular Dichroism Measurement of *Lm*-CspA. Circular dichroism (CD) measurements were performed in a J810 spectropolarimeter (Jasco) using a cell with a 1 mm path length. The CD spectra of *Lm*-CspA in 50 mM potassium phosphate buffer (pH 6.0) containing 100 mM KCl and 0.1 mM EDTA at 25 °C were measured at 0.1 nm intervals from 190 to 250 nm. The protein concentration was 50 μM, and data from 10 scans were averaged and smoothed using J810. CD data were expressed as the mean residue ellipticity (θ) in degrees square centimeters per decimole. Protein T_m values were determined from a series of CD spectra obtained at 15−80 °C.

NMR Experiments and Assignments. All NMR experiments were performed at 25 °C on Bruker Avance 500 and 800 MHz spectrometers at the Korea Basic Science Institute. Internal 2,2-dimethyl-2-silapentane-5-sulfonate was used as a chemical shift reference. *Lm*-CspA samples were prepared at a concentration of 0.8 mM in 50 mM potassium phosphate buffer containing 100 mM KCl and 0.1 mM EDTA (pH 6.0). The *Lm*-CspA-dT_7 sample was prepared by titration of 0.8 mM uniformly ^{13}C- and ^{15}N-labeled *Lm*-CspA and unlabeled dT_7 in a 1:1 ratio. For backbone assignments, HNCO, HN(CA)CO, CBCA(CO)NH, and HN(CO)CA triple-resonance spectra were recorded, and assignments of aliphatic side chains were obtained from HBHA(CO)NH, HNHA, HCCH-total correlation spectroscopy (TOCSY), and CCH-TOCSY spectra. The large resonance attributable to the water proton was suppressed by the WATERGATE pulse sequence. Nuclear Overhauser effect (NOE) distance constraints were measured from three-

dimensional $^{1}H-^{15}N$ and $^{1}H-^{13}C$ nuclear Overhauser effect spectroscopy−heteronuclear single-quantum coherence (NOESY−HSQC) spectra acquired with an 800 MHz Bruker Avance NMR spectrometer equipped with a ^{1}H-(^{13}C,^{15}N) triple-resonance probe using a mixing time of 120 ms.[30−32] Backbone assignments were confirmed on three-dimensional $^{1}H-^{15}N$ and $^{1}H-^{13}C$ NOESY−HSQC spectra. NMR spectra were processed with NMRPipe[33] and interpreted with Sparky.[34] The chemical shifts, coordinates, and NMR-derived constraints have been deposited in the Biological Magnetic Resonance Bank (entries 18679 for *Lm*-CspA-dT_7 and 18680 for free *Lm*-CspA).

Structure Determination. NOE assignments and structure calculations were accomplished using combined automated and manual methods in CYANA 2.1[35] together with dihedral (φ and ψ) constraints from chemical shifts using TALOS.[36] After seven cycles of structure calculation, a total of 100 structures were calculated using a torsion angle dynamics protocol. The structures were classified according to the final target function value, and the angle and distance violations of the best 20 structures were analyzed. CYANA structures were refined using a water refinement protocol to obtain the final structures within Crystallography and NMR System (CNS) using the topallhdg-5.3.pro/parallhdg5.3.pro force field.[37] The 20 lowest-energy structures were subjected to water refinement and further analysis with PROCHECK. The protein structure figures were generated with PyMOL (http://www.pymol.org). Final coordinates and NOE constraints have been deposited in the Protein Data Bank (PDB) as entries 2LXJ (*Lm*-CspA-dT_7) and 2LXK (free *Lm*-CspA).

Analysis of *Lm*-CspA-dT_7 Binding Using $^{15}N-^{1}H$ HSQC Spectra. Uniformly ^{15}N-labeled *Lm*-CspA for HSQC analysis was prepared at a concentration of 0.1 mM in a 9:1 (v/v) H_2O/D_2O potassium phosphate-buffered solution (50 mM, pH 6.0), containing 100 mM KCl and 0.1 mM EDTA. Chemical shift changes in the $^{1}H-^{15}N$ spectra of *Lm*-CspA were measured by titration with a dT_7 stock solution. The magnitude of the chemical shift perturbation and changes in the intensities after dT_7 binding were used to map binding site residues in *Lm*-CspA. Two-dimensional NMR titration experiments were conducted in which dT_7 was added at various protein:dT_7 ratios (1:0 to 1:1.2). Chemical shift changes of the K7, W8, F17, F27, H29, and Q59 side chains were measured using the chemical shifts of side chain protons in two-dimensional HSQC, three-dimensional HCCH-TOCSY, and CCH-TOCSY spectra.

Construction of a Binding Model of dT_7 and *Lm*-CspA. To construct a binding model of dT_7 and *Lm*-CspA, we conducted a molecular docking study and molecular dynamics (MD) simulations. The NMR structure of *Lm*-CspA bound to dT_7 was used for the initial docking structure. Using the X-ray cocomplex structures of *Bs*-CspB and nucleic acids (PDB entries 2ES2 and 3PF4)[20,38] as well as results of chemical shift changes from HSQC titration experiments, we defined binding sites and considered receptor−ligand interactions. In the X-ray cocomplex structure of *Bs*-CspB and nucleic acids, only five nucleic acids are represented by electron density. Therefore, a thymidine was prefixed to the 5′ end, and one more thymidine was appended at the 3′ end of the five nucleic acids in the X-ray structure of the *Bs*-CspB complex. Computations were performed on a Windows platform using CDOCKER, a CHARMm-based MD method for ligand docking, in Discovery Studio modeling (Accelrys Inc., San Diego, CA).[39−41] The Input Site Sphere parameter specified a sphere around the center of the binding site that was used in the CDOCKER algorithm for initial ligand placement. The MD-simulated annealing process was performed using a rigid protein and a flexible ligand. The MD simulation was conducted using the final docking structures with the Standard Dynamics Cascade Protocol in DS modeling. All *Lm*-CspA atoms, with the exception of side chains of K7, W8, F15, F17, H29, F30, and R56 in the nucleic acid-binding residues, were fixed on the basis of the chemical shift perturbation data as well as spin-relaxation data. For initial minimization, the steepest descent method was applied to a 0.1 kcal mol^{-1} $Å^{-1}$ root-mean-square energy gradient and was followed by applying a conjugate gradient method until the final convergence criterion reached 0.001 kcal mol^{-1} $Å^{-1}$ root-mean-square gradient. The entire system was then heated from 50 to 300 K in 2 ps and equilibrated at 300 K for 100 ps. One hundred conformations were collected in a 20 ps production phase at 300 K.

NMR Investigation of Backbone Dynamics. For NMR-relaxation studies of free *Lm*-CspA and the dT_7-bound complex, we performed NMR spin-relaxation experiments and analyzed R_1, R_2, and heteronuclear NOE (hNOE) NMR spectra acquired on a Bruker Avance 500 MHz spectrometer.[42−44] Longitudinal (R_1) spin-relaxation rates were obtained, and relaxation delays were 0.00200 (twice), 0.0450, 0.100, 0.200, 0.315 (twice), 0.550, 0.800, and 1.00 s. The transverse (R_2) relaxation rate was measured with relaxation delays of 0 (twice), 0.0166, 0.0333, 0.0499 (twice), 0.0666, 0.116, 0.183, and 0.283 s. The recycle delay in all R_1 and R_2 relaxation measurements was 2.5 s. The heteronuclear cross-relaxation rate was obtained from NOE experiments by interleaving pulse sequences with and without proton saturation. The recycle delay and proton saturation time in hNOE measurements were 4.5 and 3.0 s, respectively. All relaxation spectra were acquired with a ^{15}N frequency of 120 ppm and the ^{1}H carrier set coincident with the water resonance; spectral widths were 6252 and 1551 Hz in the t_2 and t_1 dimensions, respectively, with 2048 and 200 complex points in the corresponding dimensions. The data were processed with NMRPipe[33] and visualized using Sparky.[34] hNOEs were determined from the ratio of peak heights for experiments with and without proton-saturation pulses. R_1 and R_2 rates were determined by fitting the peak heights using Curvefit, available from A. Palmer at Columbia University (New York, NY) (http://biochemistry.hs.columbia.edu/labs/palmer/software/curvefit.html).

Constant-time relaxation-compensated Carr−Purcell−Meiboom−Gill (CPMG) experiments were performed under the following conditions. For 0.8 mM free *Lm*-CspA and *Lm*-CspA-dT_7 samples, spectra were collected on the Bruker Avance 500 MHz spectrometer.[45] Relaxation dispersion spectra were collected as a series of 14 two-dimensional data sets with CPMG field strengths of 50, 75, 100 (twice), 125, 150, 175, 200 (twice), 250, 325, 400, 500 (twice), 625, 750, and 1000 Hz; reference spectra were obtained by omitting the CPMG intervals in the pulse sequence. Each two-dimensional spectrum was recorded as a complex data matrix comprising 192 × 1024 points. Twenty-four scans/free induction decays were recorded using a constant time delay of 40 ms and a recycle delay of 2.0 s, resulting in a net acquisition time of approximately 3 h per data set. The intensities of cross-peaks were then converted into decay rates, R_2^{eff}, for a given field strength, υ_{cp}.[46]

dx.doi.org/10.1021/bi301641b | *Biochemistry* 2013, 52, 2492−2504

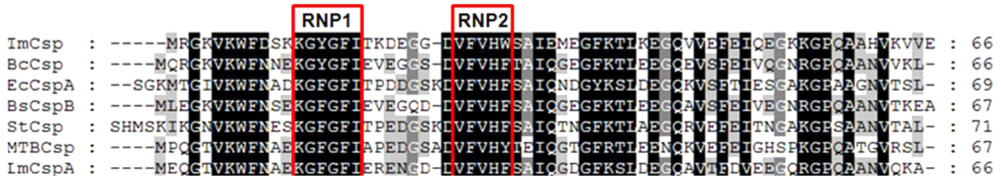

Figure 1. Sequence alignments of seven prokaryotic Csps sequences: black for 100% conserved residues, dark gray for 80% conserved residues, and light gray for >60% conserved residues.

Model-Free Analysis. Protein amide backbone dynamics were characterized by fitting ^{15}N NMR relaxation rates to one of five semiempirical forms of the spectral density function with the model-free formalism.[47,48] Spin-relaxation data were described using five models: (1) S^2 only; (2) S^2 and τ_e; (3) S^2 and R_{ex}; (4) model 2 with R_{ex}; and (5) S_f^2, S^2, and τ_e, the extended two-time scale model.[49,50] Herein, S^2 is the generalized order parameter. τ_e is the internal correlation time. S_f^2 is the fast motion order parameter with a typical correlation time of <10 ps, and R_{ex} is the additional line broadening caused by assumed two-site conformational exchange, which depends on the equilibrium site population, the rate of exchange between conformers, and chemical shift differences. Motion parameters were fit to the spin-relaxation data using FAST-Model-free with Model-Free 4.2.[49−51] The program pdbinertia and R2R1 Diffusion (http://biochemistry.hs.columbia.edu/labs/palmer/software/diffusion.html) were used to calculate the inertia tensor from the coordinates of *Lm*-CspA and the diffusion tensor from ^{15}N R_2/R_1 experimental relaxation data. The criteria for the inclusion of residues in the diffusion tensor estimate relied on the method of Tjandra et al.[52] Because R_2 values are loaded with an R_{ex} contribution, the data containing R_{ex} were excluded from the calculation of the diffusion tensor and correlation time.

During the model-free analysis, an axially symmetric rotational diffusion tensor was used; the ^{15}N chemical shift anisotropy was assumed to be −160 ppm,[53,54] and the N−H bond lengths were assumed to be 1.02 Å. For each model, 300 randomly distributed data sets were generated. Models were selected by comparing the sum-squared error of the optimal fit with the 0.05 critical value of the distribution. Where F statistics were applicable, comparisons were made using the 0.20 critical value of the distribution.

Fluorescence Quenching. Quenching of the intrinsic fluorescence of W8 in *Lm*-CspA upon binding to nucleic acids was used to determine binding constants. The binding constant of the oligonucleotide was measured on a model RF-5301PC spectrofluorophotometer. *Lm*-CspA protein (final concentration, 10 μM) was added to 50 mM potassium phosphate buffer containing 100 mM KCl and 0.1 mM EDTA (pH 6.0) at a final protein:oligonucleotide ratio of 1:10. The sample was placed in a 2 mL thermostatically controlled cuvette, and excitation and emission path lengths were set to 10 nm. The sample was excited at 290 nm, and emission spectra were recorded for light scattering effects from 300 to 500 nm. Dissociation constants (K_d) were estimated using the following equation:[55]

$$\log\left(\frac{F_0 - F}{F}\right) = \log\frac{1}{K_d} + n\log[\text{ligand}]$$

where F and F_0 are the fluorescence intensities of *Lm*-CspA in the presence and absence of ligand, respectively, and n is the number of ligand binding sites on the protein.

RESULTS

Thermostability of *Lm*-CspA and *Lm*-CspA-dT$_7$ Determined via CD Experiments. The availability of the sequences and structures of cold-shock proteins from psychrophilic to thermophilic bacteria with a high degree of similarity makes these proteins well suited for studies of thermostabilization mechanisms in thermophilic organisms.[56] Figure 1 lists the amino acid sequence of *Lm*-CspA aligned with well-studied Csps, including *Tm*-Csp, *Bc*-Csp, *Ec*-CspA, *Bs*-CspB, *St*-Csp, and *MTB*-Csp. Csps in bacteria are structurally highly conserved with a similar number of amino acids (66−77). The sequence of *Lm*-CspA was 75% identical to that of *Bs*-CspB. These proteins contain extremely well-conserved RNA-binding motifs (RNP 1 and RNP 2) marked with a red box in Figure 1, which are rich in hydrophobic, aromatic, and basic residues and are localized next to one another on the protein surface. Although these proteins share a large degree of primary sequence homology and a high degree of three-dimensional structural similarity, they display dramatic differences in thermostability.

The secondary structure and melting temperature (T_m) of *Lm*-CspA were determined from CD measurements, as shown in Figure 2. CD spectra of *Lm*-CspA showed a maximum at 200 nm and a minimum at 215 nm, which are characteristic of a β-sheet structure. Analysis of the thermal denaturation curves obtained from 15 to 80 °C showed the T_m of *Lm*-CspA to be 40 °C, indicating that *Lm*-CspA is much less thermostable than mesophilic and thermophilic Csps. The T_m of *Lm*-CspA-dT$_7$ was 52 °C, which is significantly higher than that of free *Lm*-CspA, implying that complexation with dT$_7$ stabilizes the structure of *Lm*-CspA.

Binding Affinity of Oligonucleotides for *Lm*-CspA. *Bs*-CspB reportedly has a binding preference for pyrimidine fragments and binds to single-stranded DNA containing the cold box fragment TTATTAG, Y-box fragment TATTGGT, and dT$_7$ with K_d values of 2.0 × 10^{-8}, 5.3 × 10^{-7}, and 1.8 × 10^{-9} M, respectively.[18−20] In this study, the binding affinities of various nucleoprotein complexes using potential target sequences (thymidine oligomers, heptacytosine, and Y-box and cold box fragments) were determined through titration experiments to assess the substrate specificity of nucleic acids binding to *Lm*-CspA and its variants. Variants F15A, F17A, and F27A were selected because they have hydrophobic interactions with dT$_7$ in *Bs*-CspB.[19] The binding affinity was measured using tryptophan fluorescence quenching to determine K_d. The observed K_d values for oligonucleotides dT$_5$, dT$_6$, and dT$_7$ were 10^{-6} or 10^{-7} M, as listed in Table 1. We confirmed that dT$_7$ was the strongest binding ligand, with an estimated K_d of 1.3 × 10^{-7} M at 25 °C. To assess the effect of temperature on binding affinity, we measured the binding affinities of *Lm*-CspA with dT$_7$ at 15, 25, and 35 °C. The binding affinity of dT$_7$ (5.5 × 10^{-8} M) at the lowest temperature, 15 °C, was higher than those at higher temperatures (1.3 × 10^{-7} M at 25 °C and 1.8 ×

dx.doi.org/10.1021/bi301641b | *Biochemistry* 2013, 52, 2492−2504

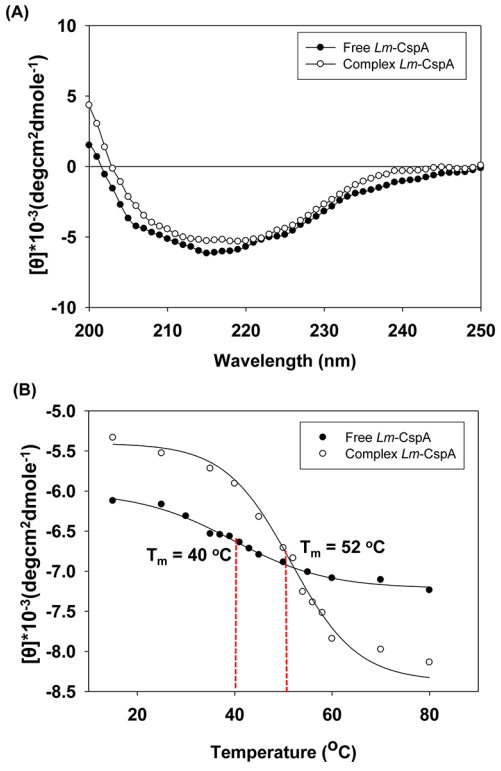

Figure 2. (A) CD spectra of free *Lm*-CspA (●) and *Lm*-CspA-dT_7 (○) in 50 mM potassium phosphate containing 100 mM KCl and 0.1 mM EDTA (pH 6.0) at 25 °C. (B) Temperature-induced change in the folding of free *Lm*-CspA and dT_7-bound *Lm*-CspA, monitored as the change in ellipticity at 215 nm.

Table 1. Dissociation Constants of the Complexes of *L. monocytogenes* Cold-Shock Protein (*Lm*-CspA) with Oligonucleotides[a]

protein	oligonucleotide (sequence)	K_d (M)
wild-type *Lm*-CspA	Y-box (TATTGGT)	7.2×10^{-6}
	cold box (TTATTAG)	2.8×10^{-6}
	dC_7 (CCCCCCC)	9.2×10^{-3}
	dT_5 (TTTTT)	8.9×10^{-6}
	dT_6 (TTTTTT)	1.4×10^{-6}
	dT_7 (TTTTTTT)	1.3×10^{-7}
	dT_8 (TTTTTTTT)	7.1×10^{-7}
Lm-CspA F15A variant	dT_7 (TTTTTTT)	1.3×10^{-5}
Lm-CspA F17A variant	dT_7 (TTTTTTT)	2.2×10^{-3}
Lm-CspA F27A variant	dT_7 (TTTTTTT)	2.5×10^{-3}

[a]All experiments were performed at 25 °C in a 10 μM solution with 50 mM potassium phosphate buffer (pH 6.0) containing 100 mM KCl and 0.1 mM EDTA.

10^{-5} M at 35 °C). This difference can be attributed to the lower flexibility of the *Lm*-CspA structure at low temperatures. The observed K_d values for several substrates at 25 °C were 7.2×10^{-6} M for TATTGGT (Y-box fragment), 2.8×10^{-6} M for TTATTAG (cold box fragment), and 9.2×10^{-3} M for dC_7. Therefore, the results demonstrated the preference of *Lm*-CspA for dT_7. The binding affinities of *Lm*-CspA variants F15A, F17A, and F27A for dT_7 were dramatically reduced, with K_d values decreasing to 1.3×10^{-5}, 2.2×10^{-3}, and 2.5×10^{-3} M, respectively, compared with that of the wild type (1.3×10^{-7} M). This result implied that residues F15, F17, and F27 are essential for binding of dT_7 to *Lm*-CspA.

Solution Structures of *Lm*-CspA and *Lm*-CspA-dT_7. The three-dimensional structures of free *Lm*-CspA and *Lm*-CspA-dT_7 were calculated on the basis of NMR constraints; NMR structural statistics for these calculations are summarized in Table 2. We included 1032 and 1009 conformational

Table 2. Structural Statistics and Mean Pairwise Root-Mean-Square Deviations for the 20 Lowest-Energy Structures of Free *L. monocytogenes* Cold-Shock Protein (*Lm*-CspA) and Complexed *Lm*-CspA (*Lm*-CspA-dT_7)

	free *Lm*-CspA	complexed *Lm*-CspA
no. of distance restraints		
total	902	871
intraresidual and sequential	431	476
medium-range	71	81
long-range	400	314
no. of dihedral angle restraints	106	112
no. of hydrogen bonds	24	26
rmsd of all the backbone residues (Å)	0.91 ± 0.13	0.72 ± 0.10
rmsd from idealized geometry		
bonds (Å)	0.0035 ± 0.00003	0.0034 ± 0.00005
angles (deg)	0.46 ± 0.007	0.45 ± 0.006
water refinement energies (kcal/mol)		
E_{NOE}	102.86 ± 12	94.22 ± 1
E_{cdih}	1.20 ± 0.009	1.29 ± 0.02
E_{elec}	−2729 ± 27	−2725 ± 25
E_{vdw}	−254 ± 6	−262 ± 6
E_{total}	−2572 ± 23	−2584 ± 24
average violations		
distance violation (d > 0.50 Å)	0	0
angle violation (θ > 5°)	0	0
Ramachandran plot statistics (%)		
residues in most favored regions	85.2	88.9
residues in additional allowed regions	14.8	11.1
residues in generously allowed regions	0	0
residues in disallowed regions	0	0

constraints in the structure calculation of free *Lm*-CspA and *Lm*-CspA-dT_7, respectively. Experimental constraints used in the calculations were as follows: (i) $^1H-^1H$ distance constraints, (ii) hydrogen bond constraints, and (iii) dihedral angle φ and ψ constraints. As shown in Figure 3, NMR spectroscopy revealed that free *Lm*-CspA forms a closed β-barrel consisting of five β-strands; two residues in these β-sheets, T5 and N62, form β-bulges, which break strand β1 into β1′ and β1″ and strand β5 into β5′ and β5″. As a result, two β-sheet surfaces, β-sheets 1 and 2, are formed by strands β1″, β2, and β3 and strands β1′, β4, β5′, and β5″, respectively. Panels A and B of Figure 3 show the protein structures of free *Lm*-CspA and *Lm*-CspA-dT_7. Five well-defined β-strands were identified in free *Lm*-CspA: β_1, E2−N10; β_2, F15−E19; β_3, D24−V28; β_4, A46−E52; and β_5, Q59−K65. These β-strands form a Greek key topology and can be arranged into two antiparallel β-pleated sheets. Two β-sheets compose a β-barrel structure stabilized by hydrophobic interactions and hydrogen bond networks within the β-sheets. The side chain groups of V6, F9,

dx.doi.org/10.1021/bi301641b | *Biochemistry* 2013, 52, 2492−2504

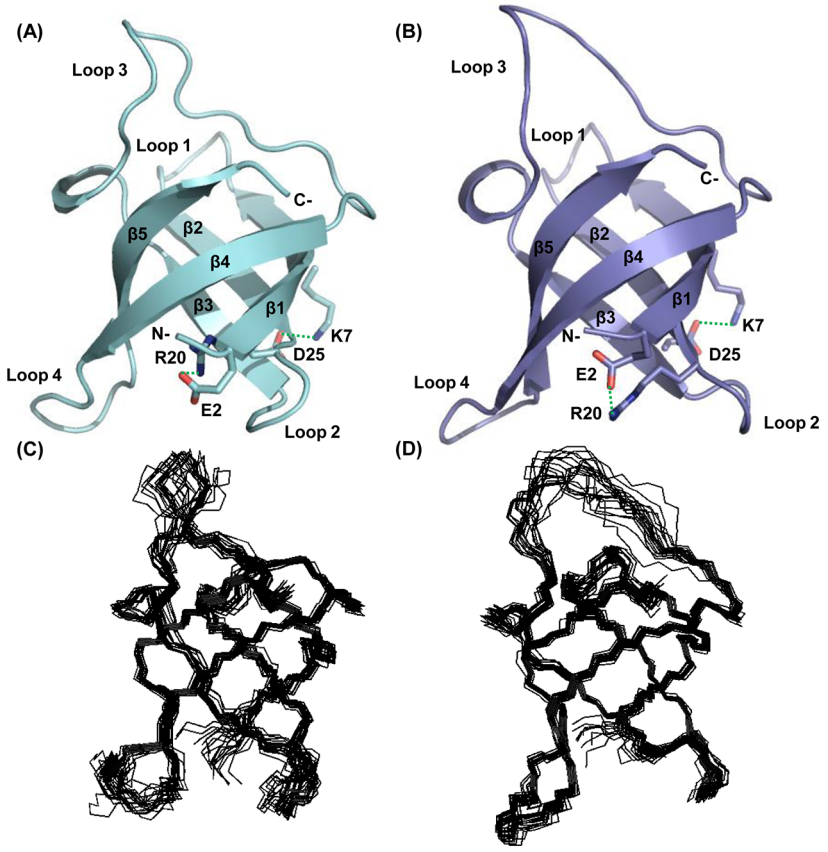

Figure 3. (A and B) Lowest-energy NMR structure of (A) free *Lm*-CspA (sky blue, PDB entry 2LXK) and (B) *Lm*-CspA-dT_7 (purple, PDB entry 2LXJ) determined using NMR spectroscopy. Hydrogen bonds are represented by dotted lines (green). (C and D) Superposition of the backbone atoms of the 20 lowest-energy structures of (C) free *Lm*-CspA and (D) *Lm*-CspA-dT_7.

I18, V26, V28, L41, V47, F49, V51, and V63 point to the interior of the β-barrel structure in *Lm*-CspA, forming a hydrophobic core. In the loop regions, only a small number of NOEs were observed, indicating that this region of the structure is disordered or mobile in solution. Loop 3 is approximately 17 residues long and contains an α-helical turn formed by F30, S31, and A32. Loop 4 encompasses six residues from E53 to P58. Another property of *Lm*-CspA is the presence of a number of solvent-exposed hydrophobic residues: W8, F15, F17, F27, and H29. These aromatic residues form a cluster of protein surfaces and are important for binding to single-stranded nucleic acids.

A comparison of free *Lm*-CspA and *Lm*-CspA-dT_7 revealed that the structure of *Lm*-CspA-dT_7 is almost invariant compared to that of the free form. *Lm*-CspA-dT_7 also consists of five very similar β-strands: β_1, E2−N10; β_2, F15−R20; β_3, D24−H29; β_4, A46−E53; and β_5, P58−K65. The difference is that β-strands β_3−β_5 in the *Lm*-CspA-dT_7 complex are longer than those of the free form. In addition, loops 3 and 4 become shorter, indicating that dT_7 binding decreases the flexibility of *Lm*-CspA and stabilizes the protein structure. Additionally, dT_7 binding shifts the dynamic equilibrium of the free form to the favorable native state, increasing T_m from 40 to 52 °C, as shown in Figure 2. Furthermore, the rings of aromatic side chains W8, F17, F27, and H29 showed movement related to base stacking with dT_7.

The backbone root-mean-square deviations (rmsds) for five β-strands and four loops between free *Lm*-CspA and dT_7-bound *Lm*-CspA were 0.83 Å (β_1), 1.07 Å (β_2), 0.27 Å (β_3), 0.54 Å (β_4), 0.20 Å (β_5), 2.19 Å (loop 1), 0.22 Å (loop 2), 2.58 Å (loop 3), and 1.18 Å (loop 4). Major structural differences between free *Lm*-CspA and *Lm*-CspA-dT_7 appeared in the lengths of surface loops 1 and 3. Panels C and D of Figure 3 show the superimpositions of 20 low-energy structures of free *Lm*-CspA and *Lm*-CspA-dT_7. The backbone rmsds for all residues from the mean structure were 0.91 ± 0.13 Å for free *Lm*-CspA and 0.72 ± 0.10 Å for *Lm*-CspA-dT_7 (Table 2). In the β-sheet-ordered regions, backbone rmsds from the mean structure were 0.40 ± 0.07 Å for free *Lm*-CspA and 0.23 ± 0.07 Å for *Lm*-CspA-dT_7. As shown in panels A and B of Figure 3, both the *Lm*-CspA structure and the structure of the complex displayed two ionic interactions: E2−R20 and K7−D25.

Chemical Shift Perturbations of *Lm*-CspA upon dT_7 Binding. We compared the backbone ^1H and ^{15}N chemical shifts of *Lm*-CspA in the presence and absence of dT_7. Because local structural rearrangements occur when a ligand binds to a protein, these chemical shift variations were analyzed by comparing the $^{15}N-^1H$ HSQC spectra of free *Lm*-CspA and *Lm*-CspA-dT_7. Figure 4A shows the overlay of the two-dimensional $^{15}N-^1H$ HSQC spectra of *Lm*-CspA and dT_7-bound *Lm*-CspA at an *Lm*-CspA:dT_7 molar ratio of 1:1. Peaks showing large chemical shift variations upon dT_7 binding are indicated by blue lines in Figure 4A. Using chemical shift perturbation data, we found that residues located at dT_7 binding sites and in the loop region showed large chemical shift changes. From this, we concluded that these residues facilitate the binding of dT_7 through direct interaction or conformational rearrangements remote from the binding

dx.doi.org/10.1021/bi301641b | *Biochemistry* 2013, 52, 2492−2504

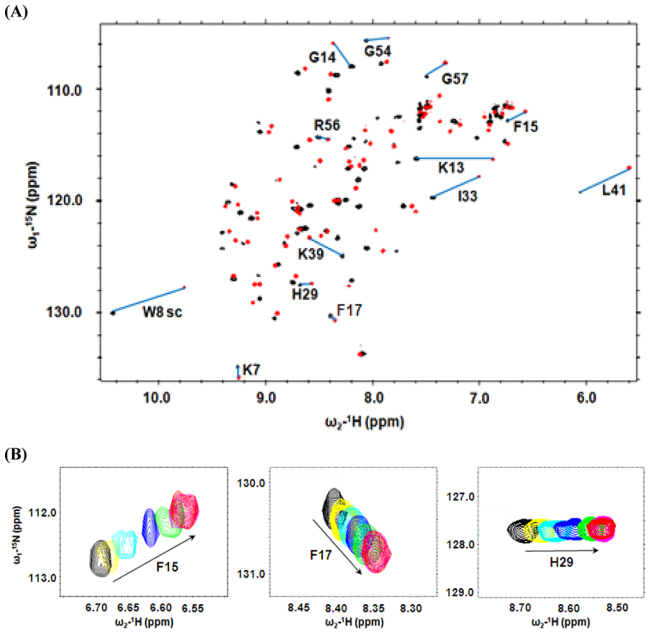

Figure 4. (A) Overlay of $^{1}H-^{15}N$ HSQC spectra of free *Lm*-CspA (black) and *Lm*-CspA-dT_7 (red) tested at a 1:1 *Lm*-CspA:dT_7 molar ratio. Protein samples (0.1 mM) were prepared in 50 mM potassium phosphate buffer containing 100 mM KCl and 0.1 mM EDTA (pH 6.0). (B) Peak traces for the dT_7 titration in the HSQC spectra showing the signal changes of *Lm*-CspA after titration with dT_7 at ratios of (a) 0:1 (black), (b) 0.1:1 (yellow), (c) 0.3:1 (sky blue), (d) 0.5:1 (blue), (e) 0.7:1 (green), (f) 1:1 (red), and (g) 1.2:1 (magenta).

interface. Figure 4B shows the peak trace of F15, F17, and H29 of *Lm*-CspA at 0.1 mM for dT_7 titration in $^{1}H-^{15}N$ HSQC spectra. The NMR signals gradually shifted in a single direction with the addition of dT_7, indicating that the rate of exchange of dT_7 between the free and bound states is faster than the NMR time scale.

The chemical shifts of side chain protons in the three-dimensional HCCH-TOCSY, CCH-TOCSY, and HSQC-NOESY spectra were measured. Chemical shift perturbation of the NH side chains was seen at K7 (from 6.776 to 6.889 ppm), Q59 (from 7.792 to 7.593 ppm), and the imidazole ring NH group in W8 (from 10.41 to 9.770 ppm). F17, F27, and H29 form a hydrophobic patch that binds dT_7, changing the chemical shift of aromatic ring protons as well. Our chemical shift perturbation data and the complex structure of *Bs*-CspB-dT_7 reported by Balbach et al.[20] suggest that the side chains of residues K7, W8, F17, F27, H29, and Q59 in *Lm*-CspA may interact with dT_7 through hydrogen bonds or hydrophobic interactions.

^{15}N NMR Relaxation Study. The dynamic properties of free *Lm*-CspA were compared with those of *Lm*-CspA-dT_7. The results of spin-relaxation experiments with free *Lm*-CspA and dT_7-bound *Lm*-CspA (at an *Lm*-CspA:dT_7 molar ratio of 1:1) are shown in Figure 5. The average R_1, R_2, and hNOE values of free *Lm*-CspA were 2.38 ± 0.061 s^{-1}, 7.23 ± 0.35 s^{-1}, and 0.58 ± 0.022 unit, respectively, whereas the corresponding values of dT_7-bound *Lm*-CspA were 2.63 ± 0.082 s^{-1}, 6.72 ± 0.24 s^{-1}, and 0.68 ± 0.039 unit, respectively. The average R_2/R_1 ratio for free *Lm*-CspA was 2.87 ± 0.27, whereas that for bound *Lm*-CspA was 2.56 ± 0.24, implying that both free *Lm*-CspA and the bound form exist as monomers. *Lm*-CspA spin-relaxation rate data revealed large R_2 values (>10 s^{-1}) for the backbone

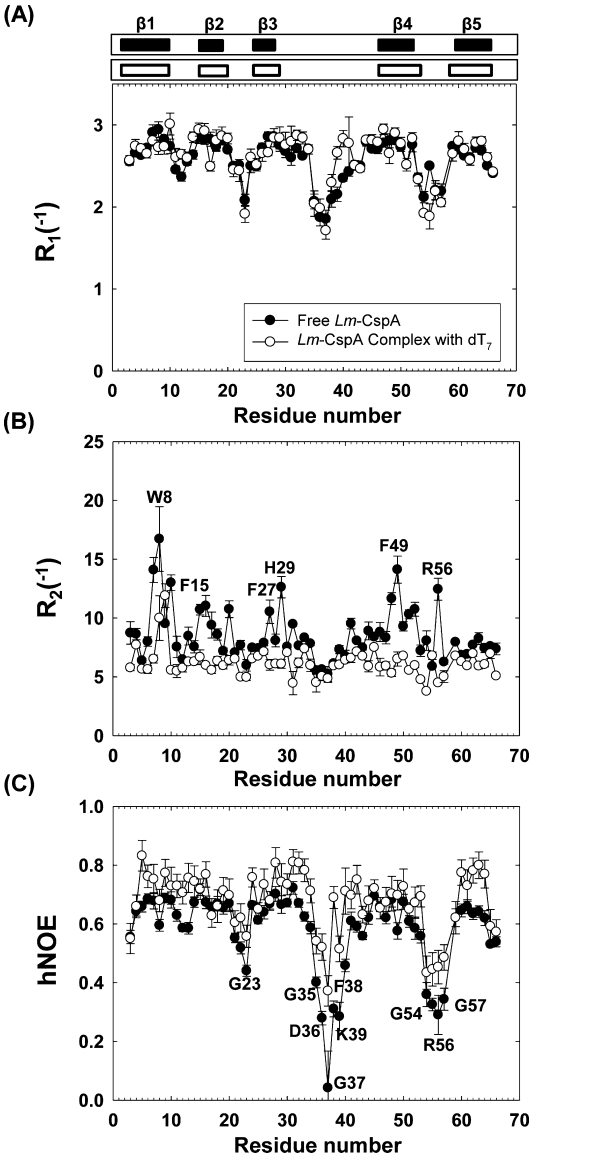

Figure 5. Comparison of R_1, R_2, and hNOE values for free *Lm*-CspA (●) and *Lm*-CspA-dT_7 (○) at pH 6.0, at a 1:1 *Lm*-CspA:dT_7 molar ratio. Filled bars represent the five *β*-strands of free *Lm*-CspA, and empty bars represent those of *Lm*-CspA-dT_7.

NH groups of K7, W8, N10, F15, G16, R20, F27, H29, T48, F49, V51, E52, and R56; these residues are excluded for calculations of the average R_2/R_1 ratio. These large R_2 values could be due to the conformational exchange (R_{ex}) of the protein on microsecond to millisecond time scales. Conformational exchanges of K7 (14.08 to 6.52 s^{-1}), W8 (16.72 to 10.00 s^{-1}), F15 (10.71 to 6.68 s^{-1}), F27 (10.54 to 6.03 s^{-1}), H29 (12.62 to 6.10 s^{-1}), and R56 (12.44 to 4.50 s^{-1}) were decreased upon dT_7 binding. This implies that the level of conformational exchange is reduced dramatically upon binding and suggests that electrostatic or hydrophobic interactions with a nucleic acid may be essential for dT_7 binding. Interestingly, F49, which forms the hydrophobic core in dT_7-bound *Lm*-CspA, exhibited a large decrease in its R_2 value (from 14.11 to 6.53 s^{-1}) because the aromatic ring of F49 moved to a suitable spatial orientation, allowing hydrophobic interactions with other residues through formation of a hydrophobic core.

dx.doi.org/10.1021/bi301641b | *Biochemistry* 2013, 52, 2492−2504

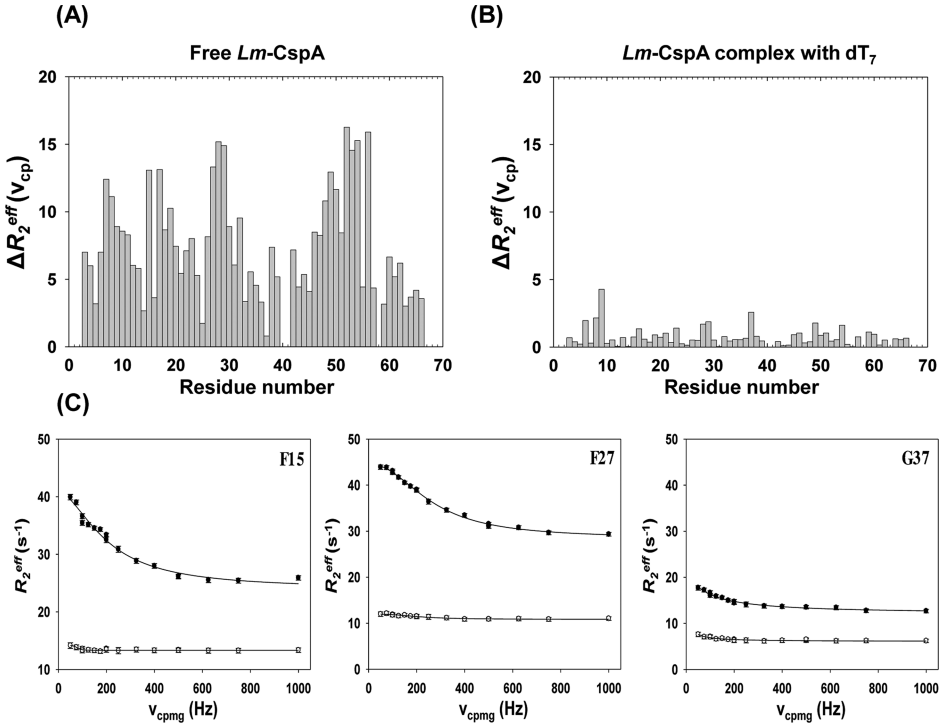

Figure 6. Chemical exchanges in (A) free *Lm*-CspA and (B) *Lm*-CspA-dT$_7$. The value $\Delta R_2^{\text{eff}}(\nu_{\text{cp}})$ was determined from the difference in measured relaxation rates, $R_2^{\text{eff}}(\nu_{\text{cp}},50\text{ Hz}) - R_2^{\text{eff}}(\nu_{\text{cp}},1000\text{ Hz})$. (C) Experimental data for free *Lm*-CspA (●) and *Lm*-CspA-dT$_7$ (○) recorded using 500 MHz NMR. Solid lines indicate fitted curves.

Residues in the flexible loop regions exhibited very low hNOEs. The average hNOE values in loop regions were 0.621 (loop 1), 0.548 (loop 2), 0.517 (loop 3), and 0.376 (loop 4). The binding of dT$_7$ to *Lm*-CspA increased the hNOE values of these loop regions to 0.750, 0.594, 0.667, and 0.455, respectively, because of the stabilization of the fast time scale motions of the loop regions in the *Lm*-CspA structure upon dT$_7$ binding. The average hNOE value was 0.58 for free *Lm*-CspA, which increased to 0.68 for the dT$_7$-bound form.

To investigate microsecond to millisecond motions in *Lm*-CspA, we performed a CPMG experiment on *Lm*-CspA and its bound form. In panels A and B of Figure 6, the differences in R_2^{eff} values are plotted as a function of amino acid sequence, because a chemical exchange at the protein backbone is evident from these differences measured at long (ν_{cp} = 50 Hz) and short (ν_{cp} = 1000 Hz) interpulse delays. ^{15}N CPMG relaxation dispersion, calculated as $\Delta R_2^{\text{eff}}(\nu_{\text{cp}}) = R_2^{\text{eff}}(\nu_{\text{cp}},50\text{ Hz}) - R_2^{\text{eff}}(\nu_{\text{cp}},1000\text{ Hz})$, revealed that the binding of dT$_7$ reduced slow time scale motion, dramatically decreasing R_{ex} values of the binding epitope and stabilizing the structure of *Lm*-CspA. The fitted experimental data at 500 MHz NMR for F15, F27, and G37 are shown in Figure 6C. F15 and F27 at the binding site in free *Lm*-CspA underwent chemical exchange on a microsecond to millisecond time scale. In contrast to those of free *Lm*-CspA, the relaxation dispersions of these residues disappeared in dT$_7$-bound *Lm*-CspA as a result of conformational stabilization. As a control, fitted data for G37 in the nonbinding site showed that the values of $R_2^{\text{eff}}(\nu_{\text{cp}})$ were invariant to CPMG pulse spacing, indicating that no conformational motion existed on this time scale. The average ΔR_2^{eff} values of free *Lm*-CspA were 7.62 s^{-1}, whereas the corresponding value of dT$_7$-bound *Lm*-CspA was 0.76 s^{-1}. In particular, the ΔR_2^{eff} values of F15 (13.08 to 0.75 s^{-1}), F17 (13.12 to 0.59 s^{-1}), H29 (14.90 to 1.88 s^{-1}), and R56 (15.90 to 1.30 s^{-1}) dramatically decreased upon dT$_7$ binding. Thus, the relaxation study provided evidence that slow time scale motions near the dT$_7$ binding site are essential for dT$_7$ binding and further indicated that dT$_7$ binding imparts structural stability on *Lm*-CspA.

Model of Binding of *Lm*-CspA and dT$_7$ Constructed on the Basis of Docking Study Results. Docking and MD simulations based on results obtained from chemical shift perturbations as well as spin-relaxation experiments helped us to construct a possible model of the binding of dT$_7$ and *Lm*-CspA. The initial structure was obtained from the NMR structure of the *Lm*-CspA-dT$_7$ complex. Upon binding, the peaks of *Lm*-CspA residues K7, W8, N10, K13, G14, F15, F27, V28, H29, F30, and R56 exhibited large chemical shift perturbations as well as decreases in conformational exchange and increases in hNOE values, as shown in Figures 4 and 5. All *Lm*-CspA atoms in the *Lm*-CspA-dT$_7$ complex were fixed with the exception of the side chains of K7, W8, N10, K13, G14, F15, F27, V28, H29, F30, and R56 in the nucleic acid-binding residues at these ligand-binding surfaces. We applied distance constraints (2.5−4.0 Å) for the interactions between the side chains of these residues and dT$_7$. Oligonucleotide dT$_7$ consists of seven nucleotides, including the first nucleotide (T1) have a 5′-phosphate group and the seventh nucleotide (T7) have a 3′-hydroxyl group in dT$_7$; the remainder successively connect to T1. The docking model and the specific interactions involved are shown in Figure 7. dT$_7$ and *Lm*-CspA interact via hydrogen bonds and tight hydrophobic connections. The side chains of the purple residues form a ligand-binding surface. *Lm*-CspA and dT$_7$ binding is dominated by hydrophobic interactions between the side chain W8, F15, F17, F27, and H29 and the bases of dT$_7$. Also, hydrogen bonds connect $N^{\varepsilon 1}$ of the imidazole ring of W8 and N^{ζ} of K7 to the oxygen group of the dT$_7$ base, O^4 of T5, and O^2 of T4. An additional hydrogen

dx.doi.org/10.1021/bi301641b | *Biochemistry* 2013, 52, 2492−2504

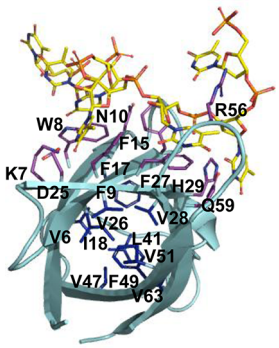

Figure 7. Overall structure of the *Lm*-CspA-dT_7 complex determined using docking studies. The binding model of dT_7 and *Lm*-CspA shows hydrogen bonding and hydrophobic interactions involving K7, W8, N10, F15, F17, D25, F27, H29, R56, and Q59 (purple). A hydrophobic core is formed by 10 residues: V6, F9, I18, V26, V28, L41, V47, F49, V51, and V63 (blue). dT_7 is represented as sticks and colored according to the CMYK scheme with the exception of carbon, which is colored yellow.

bond is formed between N^3 of T4 and $O^{\delta 2}$ of D25. $O^{\delta 1}$ of N10 interacts with N^3 of T4. Docking induced changes in the side chain orientations of these interacting residues, K7, W8, N10, F15, F17, D25, F27, H29, R56, and Q59, relative to those of the NMR structure of *Lm*-CspA-dT_7, with an average side chain rmsd of 0.87 Å. Notably, the K7, W8, and H29 side chains were considerably perturbed, with an average rmsd of 1.24 Å. The side chains of F15 and F17 did not move to any great extent; their rmsd values were 0.38 and 0.36 Å, respectively. In the case of the *Bs*-CspB-dT_6 structure, several hydrogen bonds between nucleobase groups and polar amino acids were observed; these involved N^{ζ} of K7, $N^{\varepsilon 1}$ of the imidazole ring of W8, $O^{\delta 2}$ of D25 and T4, N^{η} of R56 and T5, and $N^{\varepsilon 2}$ of Q59 and T2 and T3. Hydrophobic interactions involved residues F17, F27, H29, and F30, which form stacks with T4, T3, T2, and T6, respectively.[20] In the case of the *Bs*-CspB-nucleic acid complexes, *Bs*-CspB-rC_7 and *Bs*-CspB-dT_7,[20,38] both structures exhibited a nearly identical five-β-strand β-barrel conformation and a common mode of nucleic acid binding characterized by a highly conserved set of nucleic acid-binding subsites. Tests of the affinities of single-stranded DNA and RNA for *Bs*-CspB using tryptophan fluorescence titration revealed that the binding affinity of single-stranded RNA was significantly lower than that of single-stranded DNA.[20,38] The binding between the ligand and the protein was dominated by hydrophobic interactions of the aromatic side chain. Therefore, the hydrophobic effect of the additional methyl group of thymine seems to be responsible for the higher affinity of dT_7.

NMR-Derived Dynamics Parameters. Global and site-specific dynamics information for free *Lm*-CspA and dT_7-bound *Lm*-CspA was obtained by model-free analysis. Using an axially symmetric diffusion tensor, we found D_{II}/D_I ratios of 1.15 and 1.26 for free *Lm*-CspA and dT_7-bound *Lm*-CspA, respectively. The order parameter, S^2, describes the degree of spatial restriction of the backbone N−H bond vector in model-free analysis (Figure 8). S^2 values are indicated in color on the ribbon structure of *Lm*-CspA in Figure 9, and the R_{ex} values for the residues are shown with a larger ribbon diameter.

The S^2 values for residues near dT_7 binding sites were dramatically affected by dT_7 binding. The S^2 values for K7 and W8 increased from 0.87 ± 0.05 to 0.94 ± 0.02 and from 0.79 ± 0.04 to 0.91 ± 0.03, respectively. The average values of S^2 in β-strand regions were 0.86 (β_1), 0.91 (β_2), 0.87 (β_3), 0.86 (β_4), and 0.81 (β_5). The binding of dT_7 to *Lm*-CspA increased the S^2 values of these strand regions to 0.91, 0.94, 0.92, 0.91, and 0.92, respectively. The average S^2 values of loop regions were dramatically affected by dT_7 binding. The average values of S^2

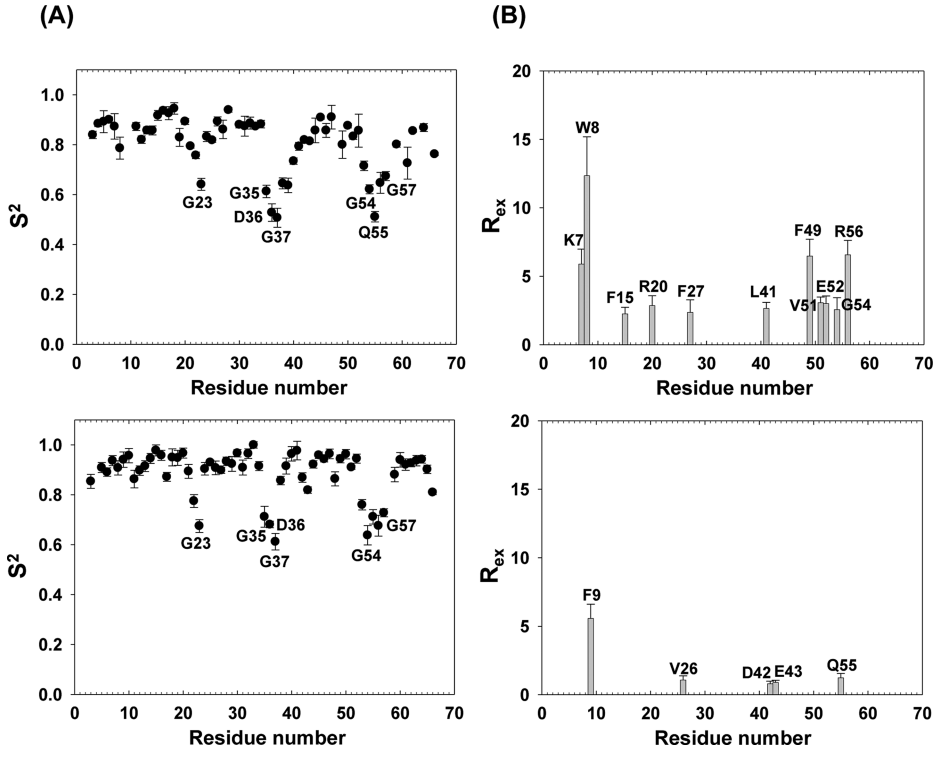

Figure 8. Optimized model-free parameters S^2 and R_{ex} for (A) free *Lm*-CspA and (B) *Lm*-CspA-dT_7 at a 1:1 *Lm*-CspA:dT_7 molar ratio.

dx.doi.org/10.1021/bi301641b | *Biochemistry* 2013, 52, 2492−2504

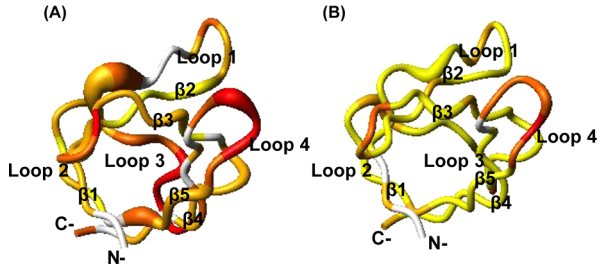

Figure 9. Spatial location of NMR-derived dynamic parameters of (A) free *Lm*-CspA and (B) *Lm*-CspA-dT_7. S^2 value ranges are indicated in various colors in tubular drawings. Residues with R_{ex} values of >0.5 s^{-1} are shown with larger ribbon diameters. Color scheme: yellow, $S^2 > 0.9$; orange, $0.8 < S^2 < 0.9$; dark orange, $0.65 < S^2 < 0.8$; and red, $S^2 < 0.65$. This figure was prepared using MolMol,[62] and the orientation of the figure is identical to that in Figure 7.

in the loop regions were 0.85 (loop 1), 0.77 (loop 2), 0.77 (loop 3), and 0.63 (loop 4). Upon dT_7 binding, these values increased to 0.90, 0.78, 0.88, and 0.69, respectively. As a result, the binding of dT_7 provided more rigidity to *Lm*-CspA by decreasing the level of fast time scale motion.

The microsecond and millisecond time scale motions were also captured in the model-free analysis. Values of R_{ex} greater than 2.0 s^{-1}, denoted with a larger ribbon diameter, are labeled in Figure 8. In free *Lm*-CspA, 11 residues showed slow conformational motions. However, the slow motions of residues K7, W8, F15, F27, and R56 near the dT_7 binding site disappeared upon dT_7 binding. F49 and V51 also exhibited R_{ex}, but the binding of dT_7 reduced the level of conformational exchange, changing the side chain orientation of F49 such that it participated with V51 in the hydrophobic core. These results are in agreement with the conformational exchange data obtained in CPMG experiments, implying that the binding of dT_7 interfered with the slow conformational motions of *Lm*-CspA and resulted in its structural stabilization. Notably, slow exchanges appeared for F9 upon binding to dT_7. F9, which forms the hydrophobic core with other hydrophobic residues in free *Lm*-CspA, was slightly exposed to the surface in *Lm*-CspA-dT_7, resulting in slow motions.

DISCUSSION AND CONCLUSIONS

The intrinsic thermostabilities of Csps from hyperthermophilic, thermophilic, mesophilic, and psychrophilic bacteria reflect the optimal growth temperatures of the corresponding bacteria. The T_m of *Lm*-CspA was approximately 40 °C, which is lower than the T_m values for the thermophilic Csps, *Tm*-Csp (~80 °C), *Bc*-Csp (~77 °C), *Ec*-CspA (~60 °C), and *Bs*-CspB (~52 °C). The NMR-derived structure of *Tm*-Csp shows a peripheral ion cluster, D20−R2−E47−K63, and a salt bridge, K6−D24.[23] *Bc*-Csp also contains extensive intramolecular ion pairing, including E21−K5−E46−R3 and K7−D25.[22] The ionic interactions within these hyperthermophilic and thermophilic Csps play central roles in their thermostability. Both mesophilic *Bs*-CspB ($T_m \approx 52$ °C) and psychrophilic *Lm*-CspA ($T_m \approx 40$ °C) contain two salt bridges, K7−D25 and K5−E19[19] and E2−R20 and K7−D25, respectively. A notable difference between mesophilic and psychrophilic Csps is the length of their β-strands: in *Bs*-CspB, β_3 (V26−A32) and β_4 (A46−E53) are longer than they are in *Lm*-CspA (β_3, D24−V28; β_4, A46−E52).[18] This difference in β-strand length appears to be an important factor in determining structural stability and accounts for the difference in T_m between mesophilic and psychrophilic Csps.

Figure 1 shows the sequence alignments of Csps. *Bs*-CspB and *Bc*-Csp are closely related in amino acid sequence and structure but differ in thermodynamic stability because the charges of *Bc*-Csp are better balanced than those of *Bs*-CspB. In particular, R3 and L66 in *Bc*-Csp contribute individually to the differences in stability.[22] The T_m of *Bc*-Csp is approximately 77 °C, 25 °C higher than that of *Bs*-CspB.[19,22] This difference in thermostability results from the electrostatic repulsion of negatively charge residues such as E3, E46, and E66 in *Bs*-CspB. In the mutagenesis experiment, the E66L mutation strongly stabilized *Bs*-CspB and increased T_m by 21 °C because this mutation removes an unfavorable electrostatic repulsion between E3 and E66.[57,58] *Lm*-CspA carries 12 negative and six positive charges at neutral pH (isoelectric point of 4.5), resulting in negative potential over the electrostatic surface. The negative potential surface centered on E19, E21, D24, and D25 in *Lm*-CspA is conserved in *Bs*-CspB and *Bc*-Csp. However, V52 in *Bs*-CspB and *Bc*-Csp is exchanged with E52 in *Lm*-CspA, extending the negatively charged surface centered on D50, E52, and E53 in *Lm*-CspA. This additional electrostatic repulsion may be another factor in the lower thermostability of *Lm*-CspA compared with that of *Bs*-CspB and *Bc*-Csp.

Fluorescence quenching experiments showed that binding of *Lm*-CspA to the single-stranded nucleic acid dT_7 was weaker ($K_d = 1.3 \times 10^{-7}$ M) compared with that of *Bs*-CspB ($K_d = 1.8 \times 10^{-9}$ M).[20] Larger structural flexibility with longer loop regions in *Lm*-CspA compared to those of *Bs*-CspB may account for this difference in binding affinity for dT_7. The highly conserved phenylalanines in Csps are important for their interactions with nucleotides. The highly conserved phenylalanines in Csps are important for their interactions with nucleotides. A mutational analysis of solvent-exposed aromatic side chains in *Bs*-CspB showed that F15A, F17A, and F27A mutations decreased the stability of *Bs*-CspB, reducing the affinity of these *Bs*-CspB variants for dT_7 by 2 orders of magnitude compared to that of wild-type *Bs*-CspB.[20] These aromatic residues are required not only for nucleic acid binding but also for conformational stability.[59] In the NMR-derived *Lm*-CspA structure, F15, F17, and F27 form a hydrophobic patch at the nucleic acid binding site of *Lm*-CspA as shown in Figure 7. The binding affinities of *Lm*-CspA variants F15A, F17A, and F27A for dT_7 were also decreased by more than 2 orders of magnitude compared to those for wild-type *Lm*-CspA, reflecting the fact that these phenyalanines occupy the dT_7 binding site of *Lm*-CspA and are essential for binding to dT_7.

The hyperthermophilic *Tm*-Csp contains 12 hydrophobic residues (V5, F8, I17, V25, V27, I32, L40, V46, F48, I50, V62, and V63) that form a hydrophobic core.[23] The mesophilic *Bs*-CspB also has a hydrophobic core formed by 12 residues (L2, V6, F9, I18, V20, V26, V28, L41, V47, F49, I51, and V63).[18] However, in *Lm*-CspA, only 10 residues (V6, F9, I18, V26, V28, L41, V47, F49, V51, and V63) form the hydrophobic core. We theorize that this difference, which might be reflected in weaker hydrophobic packing in the core of *Lm*-CspA compared with that in hyperthermophilic and mesophilic Csps, could influence the structural flexibility of *Lm*-CspA and result in a lower T_m compared to that of thermophilic Csps.

Chemical shift perturbation studies showed that the binding of dT_7 to *Lm*-CspA affects the environment of the ^{15}N and ^{1}H backbone amide resonances; ^{15}N relaxation measurements allowed us to study internal motions of the nucleic acid-binding

dx.doi.org/10.1021/bi301641b | *Biochemistry* 2013, 52, 2492−2504

epitope of *Lm*-CspA. The motions are identified by the R_{ex} term, which indicates exchanges between conformations in various chemical environments.[59] Internal motions within RNA-binding motifs RNP 1 and RNP 2 of the mesophilic counterparts of *Lm*-CspA have been addressed through ^{15}N relaxation studies of unliganded *Ec*-CspA, *Bs*-CspB, and the *Bs*-CspB-dT_7 complex.[20,60] The binding of dT_7 to *Bs*-CspB has been shown to reduce local dynamics and increase protein stability. In the case of *Lm*-CspA, as shown in Figure 5, relatively low hNOE values were observed in loop regions, implying that this part of the *Lm*-CspA structure is mobile in solution. In *Lm*-CspA, relatively lower hNOE values were observed in loop 1 (0.62) and loop 3 (0.52) compared to those of *Bs*-CspB, indicating that these mobile surface loop regions contribute to the thermostability of *Lm*-CspA.[20]

Among residues K7, W8, F15, F17, F27, H29, and R56, which are located in the dT_7-binding site of *Lm*-CspA, the average R_2 value was 12.36 ± 1.174 s^{-1} and decreased to 6.48 ± 0.586 s^{-1} upon binding dT_7, implying that slow motions are closely related to nucleic acid binding. Using a CPMG approach, the Balbach group investigated millisecond to microsecond time scale motions of *Bs*-CspB and reported the R_{ex} contributions to R_2 of the residues identified from local dynamics or global folding reactions between the folded and unfolded state.[61] In the study presented here, we also used CPMG experiments to identify chemical or conformational exchanges in *Lm*-CspA on a microsecond to millisecond time scale (see Figure 6). As found by Balbach and colleagues, we found that many residues in free *Lm*-CspA showed ΔR_2^{eff} values, implying that these residues undergo conformational or chemical exchanges in microseconds to milliseconds. However, ΔR_2^{eff} values almost disappeared in the *Lm*-CspA-dT_7 complex; notably, the ΔR_2^{eff} values of F15, F17, H29, and R56 decreased dramatically upon dT_7 binding. This report is the first to use CPMG experiments to confirm that these slow time scale motions disappear after Csp−nucleic acid binding.

Model-free analysis confirmed the importance of motions in *Lm*-CspA, as shown in Figures 8 and 9. The average order parameter value of free *Lm*-CspA was 0.81 ± 0.02, and that of the bound form was 0.88 ± 0.02, showing that dT_7 binding introduces rigidity into the *Lm*-CspA structure, especially in the loop regions. Notably, the average S^2 value in the loop 3 region, which includes the dT_7 binding residues, exhibited great flexibility in free *Lm*-CspA (0.77 ± 0.02); however, the region became more rigid upon dT_7 binding (0.88 ± 0.02). A comparative study of dynamics features between free *Lm*-CspA and *Lm*-CspA-dT_7 showed that the motions of binding site residues are essential for dT_7 binding. As a result, changes in the internal dynamics of *Lm*-CspA upon complex formation may affect the overall thermodynamics of the binding process. Structural flexibility may be required for binding to flexible single-stranded nucleic acids and for molecular chaperone functions at low temperatures.

Considering the relationship between structure and stability in Csps, we conclude that a number of salt bridges, electrostatic repulsion, the length of the loop region and β-strands, and hydrophobic core packing are likely key factors in determining the thermostability of *Lm*-CspA. Also, spin-relaxation data revealed that nucleic acid binding stabilized the native conformations of *Lm*-CspA along the dynamic equilibrium, and the slow exchanges disappeared. Therefore, *Lm*-CspA can be characterized as a flexible protein that easily accommodates nucleic acids at low temperatures.

AUTHOR INFORMATION

Corresponding Author

*Department of Bioscience and Biotechnology, Konkuk University, Seoul 143-701, South Korea. Telephone: +822-450-3421. Fax: +822-447-5987. E-mail: ymkim@konkuk.ac.kr.

Author Contributions

J.L. and K.-W.J. contributed equally as first authors.

Funding

This work was supported by Basic Science Research Program Grant 2011-0022873 and Priority Research Centers Program Grant 2012-0006686 through the National Research Foundation of Korea, funded by the Ministry of Education, Science, and Technology, and by a grant from the High Field NMR Research Program of the Korea Basic Science Institute.

Notes

The authors declare no competing financial interest.

ABBREVIATIONS

Bc, *B. caldolyticus*; *Bs*, *B. subtilis*; CD, circular dichroism; CPMG, Carr−Purcell−Meiboom−Gill; Csps, cold-shock proteins; dT_7, heptathymidine; *Ec*, *E. coli*; hNOE, heteronuclear nuclear Overhauser effect; HSQC, heteronuclear single-quantum coherence; *Lm*, *L. monocytogenes*; MD, molecular dynamics; *MTB*, *M. tuberculosis*; NMR, nuclear magnetic resonance; NOE, nuclear Overhauser effect; NOESY, nuclear Overhauser effect spectroscopy; rmsd, root-mean-square deviation; PCR, polymerase chain reaction; RNP, ribonucleoprotein; *St*, *S. typhimurium*; *Tm*, *T. maritima*; T_m, melting temperature; TOCSY, total correlation spectroscopy.

REFERENCES

(1) Inouye, M., and Phadtare, S. (2004) Cold shock response and adaptation at near-freezing temperature in microorganism. *Sci. STKE 237*, 26.

(2) Price, P. B. (2000) A habitat for psychrophiles in deep Antarctic ice. *Proc. Natl. Acad. Sci. U.S.A. 97*, 1247−1251.

(3) Weber, M. H. W., and Marahiel, A. M. (2003) Bacterial cold shock response. *Sci. Prog. 86*, 9−75.

(4) Suutari, M., and Laakso, S. (1994) Microbial fatty acids and thermal adaptation. *Crit. Rev. Microbiol. 20*, 285−328.

(5) Chattopadhyay, M. K., and Jagannadham, M. V. (2001) Maintenance of membrane fluidity in Antarctic bacteria. *Polar Biol. 24*, 386−388.

(6) Subczynski, W. K., Markowska, E., Gruszecki, W. I., and Sielewiesiuk, J. (1992) Effect of polar carotenoids on dimyristoylphosphatidylcholine membranes: A spin-label study. *Biochim. Biophys. Acta 1105*, 97−108.

(7) Purusharth, R. I., Klein, F., Sulthana, S., Jager, S., Jagannadham, M. V., Evguenieva-Hackenberg, E., Ray, M. K., and Klug, G. (2005) Exoribonuclease R interacts with endoribonuclease E and an RNA-helicase in the psychrotrophic bacterium *Pseudomonas syringae* LZ 4W. *J. Biol. Chem. 280*, 14572−14578.

(8) Al-Fageeh, M. B., and Smales, C. M. (2006) Control and regulation of the cellular responses to cold shock: The responses in yeast and mammalian system. *Biochem. J. 397*, 247−259.

(9) Thieringer, H. A., Jones, P. G., and Inouye, M. (1998) Cold shock and adaptation. *BioEssays 20*, 49−57.

(10) Gualerzi, C. O., Giuliodori, A. M., and Pon, C. L. (2003) Transcriptional and post-transcriptional control of cold-shock genes. *J. Mol. Biol. 331*, 527−539.

(11) Sönnichsen, F. D., Davies, P. L., and Sykes, B. D. (1998) NMR structural studies on antifreeze proteins. *Biochem. Cell Biol. 76*, 284−293.

(12) Jiang, W., Hou, Y., and Inouye, M. (1997) CspA, the major cold-shock protein of *Escherichia coli*, is an RNA chaperone. *J. Biol. Chem. 272*, 196−202.
(13) Bae, W., Xia, B., Inouye, M., and Severinov, K. (2000) *Escherichia Coli* CspA-family RNA chaperones are transcription antiterminators. *Proc. Natl. Acad. Sci. U.S.A. 97*, 7784−7789.
(14) Graumann, P., Wendrich, T. M., Weber, M. H., Schroder, K., and Marahiel, M. A. (1997) A family of cold-shock proteins in *Bacillus subtilis* is essential for cellular growth and for efficient protein synthesis at optimal and low temperatures. *Mol. Microbiol. 25*, 741−756.
(15) Welker, C., Bohm, G., Schurig, H., and Jaenicke, R. (1999) Cloning, overexpression, purification, and physicochemical characterization of a cold-shock protein homolog from the hyperthermophilic bacterium, *Thermotoga maritima*. *Protein Sci. 8*, 394−403.
(16) Newkirk, K., Feng, W., Jiang, W., Tejero, R., Emerson, S. D., Inouye, M., and Montelione, G. T. (1992) Solution NMR structure of the major cold-shock protein (CspA) from *Escherichia coli*: Identification of a binding epitope for DNA. *Proc. Natl. Acad. Sci. U.S.A. 91*, 5114−5118.
(17) Schindelin, H., Jiang, W., Inouye, M., and Heinemann, U. (1994) Crystal structure of CspA, the major cold-shock protein of *Escherichia coli*. *Proc. Natl. Acad. Sci. U.S.A. 91*, 5119−5123.
(18) Schnuchel, A., Wiltscheck, R., Czisch, M., Herrler, M., Willimsky, G., Graumann, P., Maragiel, M. A., and Holak, T. A. (1993) Structure in solution of the major cold-shock protein from *Bacillus subtilis*. *Nature 364*, 169−171.
(19) Max, K. E., Zeeb, M., Bienert, R., Balbach, J., and Heinemann, U. (2006) T-rich DNA single strands bind to a preformed site on the bacterial cold-shock protein *Bs*-CspB. *J. Mol. Biol. 360*, 702−714.
(20) Zeeb, M., Max, K. E., Weininger, U., Low, C., Sticht, H., and Balbach, J. (2006) Recognition of T-rich single-stranded DNA by the cold-shock protein *Bs*-CspB in solution. *Nucleic Acids Res. 34*, 4561−4571.
(21) Max, K. E., Zeeb, M., Bienert, R., Balbach, J., and Heinemann, U. (2007) Common mode of DNA binding to cold shock domains. Crystal structure of hexathymidine bound to the domain-swapped form of a major cold-shock protein from *Bacillus caldolyticus*. *FEBS J. 274*, 1265−1279.
(22) Mueller, U., Perl, D., Schmid, F. X., and Heinemann, U. (2000) Thermal stability and atomic-resolution crystal structure of the *Bacillus caldolyticus* cold-shock protein. *J. Mol. Biol. 297*, 975−988.
(23) Kremer, W., Schuler, B., Harrieder, S., Geyer, M., Gronwald, W., Welker, C., Jaenicke, R., and Kalbitzer, H. R. (2001) Solution NMR structure of the cold-shock protein from the hyperthermophilic bacterium *Thermotoga maritima*. *Eur. J. Biochem. 268*, 2527−2539.
(24) Morgan, H. P., Wear, M. A., McNae, I., Gallagher, M. P., and Walkinshaw, M. D. (2009) Crystallization and X-ray structure of cold-shock protein E from *Salmonella typhimurium*. *Acta Crystallogr. F65*, 1240−1245.
(25) D'Auria, G., Esposito, C., Falcigno, L., Calvanese, L., Iaccarino, E., Ruggiero, A., Pedone, C., Pedone, E., and Berisio, R. (2010) Dynamical properties of cold-shock protein A from *Mycobacterium tuberculosis*. *Biochem. Biophys. Res. Commun. 402*, 693−698.
(26) Linnen, M. J., Mascola, L., Lou, X. D., Goulet, V., May, S., Salminen, C., Hird, D. W., Yonekura, L., Hayes, P., Weaver, R., Audurier, A., Plikaytis, B. D., Fannin, S. L., Kleks, A., and Broome, C. V. (1998) Epidemic Listeriosis associated with Mexican-style cheese. *N. Engl. J. Med. 319*, 823−828.
(27) Darrell, O. B., Bassam, A. A., and Brian, J. W. (1996) Cold stress proteins induced in *Listeria monocytogenes* in response to temperature downshock and growth at low temperature. *Appl. Environ. Microbiol. 62*, 1116−1119.
(28) Glaser, P., Frangeul, L., Buchrieser, C., Rusniok, C., Amend, A., Baquero, F., Berche, P., Bloecker, H., Brandt, P., Chakraborty, T., Charbit, A., Chetouani, F., Couvé, E., de Daruvar, A., Dehoux, P., Domann, E., Domínguez-Bernal, G., Duchaud, E., Durant, L., Dussurget, O., Entian, K. D., Fsihi, H., García-del, P. F., Garrido, P., Gautier, L., Goebel, W., Gómez-López, N., Hain, T., Hauf, J., Jackson, D., Jones, L. M., Kaerst, U., Kreft, J., Kuhn, M., Kunst, F., Kurapkat, G., Madueno, E., Maitournam, A., Vicente, J. M., Ng, E., Nedjari, H., Nordsiek, G., Novella, S., de Pablos, B., Pérez-Diaz, J. C., Purcell, R., Remmel, B., Rose, M., Schlueter, T., Simoes, N., Tierrez, A., Vázquez-Boland, J. A., Voss, H., Wehland, J., and Cossart, P. (2001) Comparative genomics of *Listeria* species. *Science 294*, 849−851.
(29) Birnboim, H. C., and Doly, J. (1979) A rapid alkaline extraction procedure for screening recombinant plasmid DNA. *Nucleic Acids Res. 7*, 1513−1523.
(30) Sattler, M., Schleucher, C., and Griesinger, C. (1999) Heteronuclear multi-dimensional NMR experiments for the structure determination of proteins in solution employing pulsed field gradients. *Prog. Nucl. Magn. Reson. Spectrosc. 34*, 93−158.
(31) Yamazaki, T., Lee, W., Arrowsmith, C. H., Muhandiram, D. R., and Kay, L. E. (1994) A suite of triple resonance NMR experiments for the backbone assignment of ^{15}N, ^{13}C, ^{2}H labeled protein with high sensitivity. *J. Am. Chem. Soc. 116*, 11655−11666.
(32) Vuister, G. W., and Bax, A. (1993) Measurement of two- and three-bond proton to methyl-carbon J couplings in proteins uniformly enriched with ^{13}C. *J. Magn. Reson., Ser. B 102*, 228−231.
(33) Delaglio, F., Grzesiak, S., Vuister, G. W., Zhu, G., Pfeifer, J., and Bax, A. (1995) NMRPipe: A multidimensional spectral processing system based on UNIX pipes. *J. Biomol. NMR 6*, 277−293.
(34) Goddard, T. D., and Kneller, D. G. (2008) *SPARKY 3*, University of California, San Francisco.
(35) Güntert, P., and Wüthrich, K. (1991) Improved efficiency of protein structure calculations from NMR data using program DIANA with redundant dihedral angle constraints. *J. Biomol. NMR 1*, 447−456.
(36) Cornilescu, G., Delaglio, F., and Bax, A. (1999) Protein backbone angle restraints from searching a database for chemical shift and sequence homology. *J. Biomol. NMR 13*, 289−302.
(37) Linge, J. P., Williams, M. A., Spronk, C. A., Bonvin, A. M., and Nilges, M. (2003) Refinement of protein structures in explicit solvent. *Proteins 50*, 496−506.
(38) Sachs, R., Max, K. E. A., Heinemann, U., and Balbach, J. (2012) RNA single strands bind to a conserved surface of the major cold-shock protein in crystals and solution. *RNA 18*, 65−76.
(39) Wu, G., Robertson, D. H., Brooks, C. L., III, and Vieth, M. A. (2003) Detailed analysis of grid-based molecular docking: A case study of CDOCKER-A CHARMm-based MD docking algorithm. *J. Comput. Chem. 24*, 1549−1562.
(40) Vieth, M., Hirst, J. D., Kolinski, A., and Brooks, C. L. (1998) Assessing energy functions for flexible docking. *J. Comput. Chem. 19*, 1612−1622.
(41) Vieth, M., Hirst, J. D., Dominy, B. N., Daigler, H., and Brooks, C. L. (1998) Assessing search strategies for flexible docking. *J. Comput. Chem. 19*, 1623−1631.
(42) Kordel, J., Skelton, N. J., Akke, M., Palmer, A. G., III, and Chazin, W. J. (1992) Backbone dynamics of calcium-loaded calbindin D9k studied by two dimensional proton-detected ^{15}N NMR spectroscopy. *Biochemistry 31*, 4856−4866.
(43) Skelton, N. J., Palmer, A. G., III, Akke, M., Kordel, J., Rance, M., and Chazin, W. J. (1993) Practical aspects of two-dimensional proton-detected ^{15}N spin relaxation measurements. *J. Magn. Reson., Ser. B 102*, 253−264.
(44) Kay, L. E., Keifer, P., and Saarinen, T. (1992) Pure absorption gradient enhanced heteronuclear single quantum correlation spectroscopy with improved sensitivity. *J. Am. Chem. Soc. 114*, 10663−10665.
(45) Tollinger, M., Skrynnikov, N. R., Mulder, F. A. A., Forman-Kay, J. D., and Kay, L. E. (2001) Slow dynamics in folded and unfolded states of an SH3 domain. *J. Am. Chem. Soc. 123*, 11341−11352.
(46) Mulder, F. A. A., Skrynnikov, N. R., Hon, B., Dahlquist, F. W., and Kay, L. E. (2001) Measurement of slow (μs-ms) time scale dynamics in protein side chains by ^{15}N relaxation dispersion NMR spectroscopy: Application to Asn and Gln residues in a cavity mutant of T4 lysozyme. *J. Am. Chem. Soc. 123*, 967−975.
(47) Lipari, G., and Szabo, A. (1982) Model-free approach to the interpretation of nuclear magnetic resonance relaxation in macromolecules. 1. Theory and range of validity. *J. Am. Chem. Soc. 104*, 4546−4559.

(48) Lipari, G., and Szabo, A. (1982) Model-free approach to the interpretation of nuclear magnetic resonance relaxation in macromolecules. 2. Analysis of experimental results. *J. Am. Chem. Soc. 104*, 4559−4570.
(49) Clore, G. M., Szabo, A., Bax, A., Kay, L. E., Driscoll, P. C., and Gronenborn, A. M. (1990) Deviations from the simple two-parameter model-free approach to the interpretation of ^{15}N nuclear magnetic relaxation of proteins. *J. Am. Chem. Soc. 112*, 4989−4991.
(50) Palmer, A. G., III, Rance, M., and Wright, P. E. (1991) Intramolecular motions of a zinc finger DNA-binding domain from Xfin characterized by proton detected natural abundance ^{13}C heteronuclear NMR spectroscopy. *J. Am. Chem. Soc. 113*, 4371−4380.
(51) Cole, R., and Loria, J. P. (2003) Fast-model free: A program for rapid automated analysis of solution NMR spin-relaxation data. *J. Biomol. NMR 26*, 203−213.
(52) Tjandra, N., Feller, S. E., Pastor, R. W., and Bax, A. (1995) Rotational diffusion anisotropy of human ubiquitin from ^{15}N NMR relaxation. *J. Am. Chem. Soc. 117*, 12562−12566.
(53) Hiyama, Y., Niu, C.-H., Silverton, J. V., Bavoso, A., and Torchia, D. A. (1988) Determination of ^{15}N chemical shift tensor via ^{15}N-^{2}H dipolar coupling in Boc-glycylglycyl [^{15}N glycine] benzyl ester. *J. Am. Chem. Soc. 110*, 2378−2383.
(54) Fairbrother, W. J., Liu, J., Pisacane, P. I., Sliwkowski, M. X., and Palmer, A. G., III (1998) Backbone dynamics of the EGF-like domain of heregulinalpha. *J. Mol. Biol. 279*, 1149−1161.
(55) Jaenicke, R., Schurig, H., Beaucamp, N., and Ostendorp, R. (1996) Structure and stability of hyperstable proteins: Glycolytic enzymes from hyperthermophilic bacterium *Thermotoga maritima*. *Adv. Protein Chem. 48*, 181−269.
(56) Makhatadze, G. I., Loladze, V. V., Gribenko, A. V., and Lopez, M. M. (2004) Mechanism of Thermostabilization in a Designed Cold Shock Protein with Optimized Surface Electrostatic Interaction. *J. Mol. Biol. 336*, 929−942.
(57) Perl, D., Mueller, U., Heinemann, U., and Schmid, F. X. (2000) Two exposed amino acid residues confer thermosatility on a cold shock protein. *Nat. Struct. Biol. 7*, 380−383.
(58) Zeeb, M., and Balbach, J. (2003) Single-stranded DNA binding of the cold-shock protein CspB from *Bacillus subtilis*: NMR mapping and mutational characterization. *Protein Sci. 12*, 112−123.
(59) Long, D., and Yang, D. (2010) Millisecond time scale dynamics of human liver fatty acid binding protein: Testing of its relevance to the ligand entry process. *Biophys. J. 98*, 3054−3061.
(60) Feng, W., Tejero, R., Zimmerman, D. E., Inouye, M., and Montelione, G. T. (1998) Solution NMR structure and backbone dynamics of the major cold-shock protein (CspA) from *Escherichia coli*: Evidence for conformational dynamics in the single-stranded RNA-binding site. *Biochemistry 37*, 10881−10896.
(61) Zeeb, M., and Balbach, J. (2005) NMR spectroscopic characterization of millisecond protein folding by transverse relaxation dispersion measurements. *J. Am. Chem. Soc. 127*, 13207−13212.
(62) Koradi, R., Billeter, M., and Wuthrich, K. (1996) MOLMOL: A program for display and analysis of macromolecular structures. *J. Mol. Graphics 14*, 51−55.